

Forms and sand transport in shallow hydraulic fractures in residual soil

Lawrence C. Murdoch, James R. Richardson, Qingfeng Tan, Shaun C. Malin, and Cedric Fairbanks

Abstract: Four sand-filled hydraulic fractures were created at a depth of 1.5 m, and the vicinities of the fractures were excavated and mapped in detail. All the fractures were shaped like slightly asymmetric saucers between 4.5 and 7.0 m across that were roughly flat-lying in their centers and curved upward to dip between 10° and 15° along their peripheries. Three different colors of sand were injected in sequence to trace the relative ages of the sand in the fracture. The first sand to be injected remained in the vicinity of the injection casing, whereas the last sand moved rapidly to the leading edge. Sand transport occurred through localized, channel-like pathways that extended from the injection casing and then branched into multiple paths as they approached the leading edge. At least four branching pathways of different ages were identified in one fracture, suggesting that this represents a fundamental mechanism of sand transport in these shallow fractures. A theoretical model was developed by adapting Franc2d, a code well-known in structural mechanics, to predict the propagation paths of curved hydraulic fractures at shallow depths. The model predicts fracture forms that are remarkably similar to those in field exposures when properties typical of field conditions are used.

Key words: hydraulic fracture, field test, mechanics, modeling.

Résumé : Quatre fractures hydrauliques remplies de sable ont été créées à une profondeur de 1,5 m; les alentours des fractures ont été excavés et des cartographies détaillées en ont été exécutées. Toutes les fractures avaient la forme de soucoupes légèrement asymétriques entre 4,5 m et 7,0 m en travers avec les centres à peu près aplatis, courbées vers le haut et s'inclinant entre 10° et 15° le long de leurs périphéries. Des sables de trois différentes couleurs ont été injectés les uns à la suite des autres pour indiquer les âges relatifs du sable dans la fracture. Le premier sable à être injecté est resté dans le voisinage du tuyau d'injection, alors que le dernier sable a cheminé rapidement vers l'arête en progression. Le transport du sable s'est produit à travers des cheminements localisés comme des canaux qui s'étendaient à partir du tuyau d'injection et ensuite se branchaient à de multiples cheminements lorsqu'ils s'approchaient de l'arête en progression. Au moins quatre cheminements de branchements de différents âges ont été identifiés dans une fracture, ce qui suggérerait que cette observation représentait un mécanisme fondamental de transport de sable dans ces fractures peu profondes. On a développé un modèle théorique en adaptant Franc2d, un code bien connu en mécanique des structures, pour prédire les cheminements de la propagation des fractures hydrauliques courbées à faibles profondeurs. Le modèle prédit les formes de la fracture qui sont remarquablement semblables aux observations sur le terrain lorsque des propriétés typiques des conditions sur le terrain sont utilisées.

Mots clés : fracture hydraulique, essai sur le terrain, mécanique, modélisation.

[Traduit par la Rédaction]

Introduction

Hydraulic fracturing is widely used to improve the performance of wells that serve a variety of applications, from the production of oil from reservoirs to the removal of contaminants from aquifers (Murdoch et al. 1994; Baker and Leach 1995; Valko and Economides 1995; Bradner and Murdoch 2005). Techniques for fracturing oil reservoirs have been

used in the petroleum industry for more than 50 years to improve recovery (Gidley et al. 1989), and during the past 15 years hydraulic fracturing has been developed for use in near-surface applications for environmental remediation purposes (Murdoch et al. 1994; Murdoch 2000; Wong and Alfaro 2001; Murdoch and Slack 2002).

Hydraulic fractures are created by pumping a fluid into a borehole in a geologic formation until a critical pressure is

Received 10 June 2005. Accepted 27 February 2006. Published on the NRC Research Press Web site at <http://cgj.nrc.ca/> on 6 November 2006.

L.C. Murdoch.¹ Geological Sciences Department, Clemson University, 340 Brackett Hall, Clemson, SC 29634, USA.

J.R. Richardson. FRx Inc., P.O. Box 498292, Cincinnati, OH 45249, USA.

Q. Tan. URS Corporation, 5301 77 Center Drive, Suite 41, Charlotte, NC 29262, USA.

S.C. Malin. Advent Environmental, 498 Wando Park Blvd., Suite 500, Mt. Pleasant, SC 29464, USA.

C. Fairbanks. Civil Engineering Department, Clemson University, 109 Lowry Hall, Clemson, SC 29634, USA.

¹Corresponding author (e-mail: lmurdoch@clemson.edu).

achieved and a fracture is initiated. The fracture dilates and propagates away from the borehole as injection continues. Sand is commonly injected as a slurry to prop open the fracture and create a permeable layer to increase well performance (Howard and Fast 1970; Bradner and Murdoch 2005). In some environmental applications, granules of reactive compounds are used as a proppant to create fractures for specialized applications (Murdoch et al. 1994; Murdoch and Chen 1997; Murdoch and Slack 2002).

Fracture form and the distribution of proppant determine the effectiveness of a hydraulic fracture for a particular application. *Form* is the shape, orientation, and thickness of a fracture. The forms of hydraulic fractures created at shallow depths are known from studies where the vicinity of fractures was excavated or explored using split-spoon sampling (Murdoch 1991, 1995; Wong and Alfaro 2001; Murdoch and Slack 2002). In general, the form ranges from a roughly flat-lying, nearly circular feature to a steeply dipping sheet. The typical form of many shallow hydraulic fractures is a flat-lying to gently dipping feature that dips back toward the initiating borehole to create a surface shaped like a gently curved, asymmetric bowl (Frere and Baker 1995; Murdoch 1995; Wong and Alfaro 2001; Murdoch and Slack 2002). Some hydraulic fractures are nearly vertical, however, and this form may be unsuitable for some applications, so understanding controls on fracture form has useful applications.

Fracture form appears to result from interactions between subsurface conditions at the site and the processes used to create the fracture. In particular, the in situ state of stress and material properties, such as elastic modulus and fracture toughness, appear to be particularly important (Murdoch 1995). The presence of geologic layering (e.g., bedding, foliation) may influence form by causing a hydraulic fracture to preferentially follow the layering (Murdoch 1995). Process variables, such as the viscosity of the slurry or the injection rate, may also affect form by influencing the pressure distribution within a fracture (Pollard and Holzhausen 1979).

Theoretical models describing the growth and form of shallow hydraulic fractures are limited. Recent analyses (Murdoch 2002; Savitski and Detournay 2002; Zhang et al. 2002) predict the aperture distribution for shallow, flat-lying hydraulic fractures. These analyses give results that resemble field observations of uplift and thickness of sand in fractures that are essentially axisymmetric and horizontal. These analyses assume the fracture remains in a horizontal plane, however, and they are unable to predict the growth of shallow hydraulic fractures that curve upward. Pollard and Holzhausen (1979) used an analysis of static fractures to show that mechanical interactions with the ground surface should cause the fractures to curve upward, but an analysis that predicts the form resulting from this interaction has yet to be used to explain field observations.

The distribution of granules of solid proppant affects the properties of the resulting fracture. The thickness and distribution of a proppant affect the transmissivity of a fracture used to increase well performance (Bradner and Murdoch 2005), and they are also fundamental to designing applications where the proppant is a reactive chemical used to enhance remediation. It is clear that significant volumes of proppant can be delivered to the subsurface using hydraulic fracturing, but it is less clear how to predict the mi-

gration and ultimate location of proppants delivered using this method.

Most previous field studies of hydraulic fractures created at shallow depths were done in silty clay glacial tills (Murdoch 1995; Wong and Alfaro 2001; Murdoch and Slack 2002). Silty saprolite underlies much of the Piedmont region of the eastern United States, and hydraulic fractures should be suited to improving remediation efforts in this material. The forms of hydraulic fractures in shallow saprolite have been reported briefly by Frere and Baker (1995), and they seem to resemble forms observed in glacial tills.

The primary objective of this investigation is to describe the forms of hydraulic fractures in saprolite and compare them with the forms created in other geologic materials. A theoretical model of hydraulic fracture propagation is outlined and used to explain observed fracture forms. Another objective is to evaluate the feasibility of tracing the movement of sand within a hydraulic fracture to confirm, modify, or develop new concepts for explaining proppant transport.

Methods

The field site for this study is on the Simpson Agricultural Experimental Station, approximately 5 km east of Pendleton, Anderson County, South Carolina. The study site was used for pasture prior to this experimental program, and there is no evidence the area was disturbed below plow depth before hydraulic fractures were created.

Geology and material properties

The site is underlain by the Caesar's Head granite, a light gray, medium-grained, discontinuously banded to nonbanded biotite granitoid gneiss or gneissic granitoid (Nelson et al. 1998). The granitoid is strongly weathered to saprolite at depths shallower than 10 m. Relic structure in the saprolite gives way to massive, reddish, sandy, clayey silt above approximately 2.5 m depth. This is the B horizon in the soil profile.

The contact between the saprolite and B horizon is irregular, ranging in depth from 1.5 to 3.0 m, with 2.5 m a typical value. Hydraulic fractures were created in the B horizon, slightly above the underlying contact with saprolite.

Samples of the B horizon and saprolite were analyzed in the laboratory, and field tests were also conducted to characterize the subsurface where the fractures were created (Table 1) (Richardson 2003). Grain sizes range from clay to sand in both saprolite and B-horizon materials. The B-horizon material contains mostly fine-grained sand to silt with lesser amounts of clay and sand (SM to MH). In contrast, saprolite contains mostly fine-grained sand with lesser amounts of silt-sized grains (SM). Both materials are poorly sorted, with uniformity coefficients ($C_u = D_{60}/D_{10}$) of 400 or larger in the B horizon and from 27 to more than 2000 in the saprolite.

Unconsolidated-undrained triaxial tests were conducted on four cylindrical subsamples taken from block samples. The total shear stress at failure was 34 kPa (5 psi), and the undrained angle of friction was $\phi = 32^\circ$, at normal stresses less than 170 kPa (25 psi). At greater normal stress, in the range of 170–275 kPa, the total shear stress at failure increased to 110 kPa (16 psi) and ϕ decreased to 10° .

Table 1. Soil properties at the study site.

Depth (m)	Bulk				Moisture content	Degree of saturation	Fines content (by mass <0.075 mm)	Pocket penetrometer (tsf) ^d	USCS ^b	Color of wet fines ^c	Soil horizon
	density (kg/m ³)	Porosity	Dry unit weight (kg/m ³)	Moisture content							
0.3	1499	0.41	1837	0.20	0.70	0.41	3.00	Silty sand, SM	Dark reddish brown, 5YR 3/4	A	
0.6	1109	0.56	1265	0.23	0.41	0.48	4.10	Silty sand to sandy silt, SM to MH	Red to dark red, 2.5YR 3/6 to 2.5YR 4/8	A, B	
0.9	1529	0.40	1313	0.31	0.77	0.52				B	
1.2	1419	0.44		0.31	0.70					B	
1.5	1459	0.43	1160	0.39	0.92	0.30	4.00			B	
1.8	1409	0.45		0.44	0.99					B	
2.1	1489	0.42	1043	0.40	0.96	0.27	3.60			B	
2.3	1329	0.48	1446	0.47	0.98	0.20	3.50			B, saprolite	
2.6	1319	0.48	1344	0.34	0.70	0.36	3.64	Silty sand, SM	Yellowish red, 5YR 4/6	Saprolite	
2.9	1209	0.52	278	0.43	0.82	0.13	0.44			Saprolite	
Avg.	1377	0.46		0.35	0.80						
SD	136	0.05		0.09	0.18						

^atsf, t/ft². 1 tsf = 95.76 kPa.^bUnified Soil Classification System.^cBased on the Munsell soil color charts.

Stress increased roughly linearly with strain in the triaxial tests at strain less than 0.005, and the modulus of elasticity was estimated as the slope of this part of the stress–strain curve. Modulus values increased from 24 to 48 MPa (3500 to 7000 psi) as confining stress increased from 14 to 140 kPa (2 to 20 psi). Saprolite was too friable to obtain block samples, so the elastic modulus of saprolite could not be measured.

The average hydraulic conductivity of three tests in saprolite at 3 m below the ground surface is 2.4×10^{-5} m/s, and the range is 0.8×10^{-5} to 3.5×10^{-5} m/s, according to data obtained using a Guelph permeameter. Five tests were conducted in the B horizon at depths ranging from 0.6 to 2.0 m below the ground surface. Flow rates during these tests were slower than the resolution of the permeameter, suggesting the hydraulic conductivity of the B horizon is 10^{-9} m/s or less. The results of the permeameter testing suggest that there is a contrast of three to four orders of magnitude between the in situ hydraulic conductivity of the B horizon and that of the saprolite. It is possible that natural fractures or weathered veins exist in the B horizon that would increase the effective hydraulic conductivity of regions larger than those affected by the in situ permeameter. Sowers and Richardson (1982) summarized results of many permeability tests in B-horizon material at other sites in the Piedmont, and their results indicate hydraulic conductivities are typically in the range of 10^{-7} to 10^{-8} m/s.

In situ stress at the site was estimated by analyzing pressure logs from hydraulic fractures created by injecting a few tens of millilitres of water. Fifteen of these in situ stress tests were conducted by Malin (2005) at various locations near the test site. Results indicate that the mean values of horizontal stress range from 65 to 120 kPa in the depth range of 0.9–1.5 m. The horizontal stress was always greater than the vertical stress, with a mean coefficient of earth pressure at rest K_0 of 4.7.

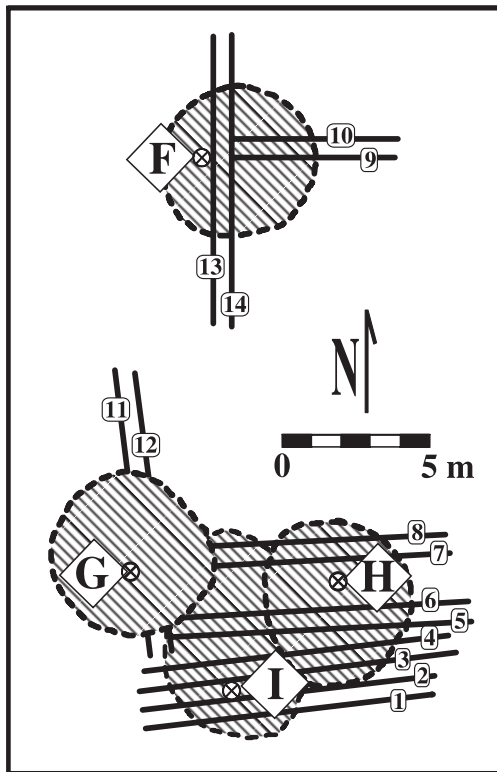
In situ stresses were also estimated using a flat-blade dilatometer. Two measurements were made and indicate that K_0 ranges from 3.0 to 3.5 at depths from 0.9 to 1.5 m. It appears that the horizontal stress is several times greater than the vertical stress in the B horizon where the hydraulic fractures were created. At greater depths in the saprolite, measurements with the dilatometer suggest that K_0 is less than 1.0.

Hydraulic fracturing

The four hydraulic fractures used for this research were created in February and March of 2002. Fractures were created by pushing a steel casing capped with a point to a depth of 1.5 m, and then advancing the point a few centimetres below the bottom of the pipe. A water jet was used to cut a horizontal starter notch at the bottom of the casing. Guar gum gel was injected into the casing, creating a fracture that started at the notch and propagated away from the casing. Sand was mixed with the gel to create a slurry that was injected into the fracture during propagation (Gidley et al. 1989).

Procedures used for this project were the same as methods in common practice used to create fractures (Murdoch et al. 1994; Murdoch and Slack 2002; Richardson 2003), with one notable exception. Sand (10/30 mesh sand sold for filter-

Fig. 1. Map of lateral extent (hatched) of fractures F, G, H, and I. Traces of trench faces 1–14 in bold lines. ⊗, injection casing.



pack applications) of three different colors (red, white (natural), and blue) was injected sequentially into the fractures. Typically only naturally colored sand is used, but we used the different colors to indicate the relative time when sand was injected.

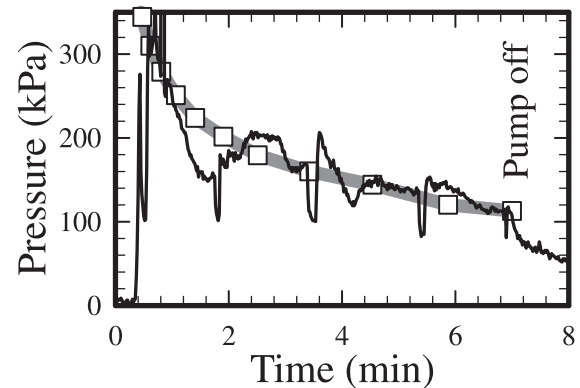
The sand was colored with Rust-Oleum® marking paint, which dries quickly after application and coats individual grains distinctly without causing the grains to cluster or clump together. Between 5 and 10 applications of paint were used to thoroughly color the sand without significantly affecting the bulk density.

A total of 250 kg of sand was injected into each fracture in the following amounts: 22 kg red, 160 kg white, and 68 kg blue. The colors were injected sequentially during continuous flow to the fracture. The transition between colors was as sharp as possible, but we expect that during each color change roughly 20 kg of sand colors were mixed together in the surface equipment prior to injection. The sand was mixed with guar gum gel mixed at 5.4 g/L (4.5 lb/100 gal) and crosslinked with borate. Breaker was omitted from the gel because it was unnecessary.

Field monitoring and mapping

The fracturing process was monitored by recording the injection pressure as a function of time and by measuring the net vertical displacement (uplift) of the ground surface. Uplift was measured by surveying an array of fixed stakes using a leveling telescope. Measurements with a vertical accuracy of 0.5 mm were made at 25 locations positioned in a radial array around the borehole. Slurry was sampled periodically from the injection hose and analyzed to determine sand loading (ratio of bulk volume of sand to total volume of

Fig. 2. Observed (solid line) and predicted (heavy gray line with open squares) injection pressure for fracture H.



slurry) and color fractions as functions of time (Richardson 2003).

Excavation of the fractures was conducted several weeks after the conclusion of fracturing activities. Two fractures (G and F) were exposed with one trench along their major axes and another trench perpendicular to it, forming a T pattern (Fig. 1). Two other fractures (H and I) were exposed using several parallel trenches, exposing the fractures as traces on serial cross sections. Fracture traces on all the trench faces were mapped onto transparent film. The upper and lower contact between sand and wall material were traced onto the film and the color of the sand in the fracture was recorded. The overburden was removed to expose fracture surfaces at several locations after the trench faces were mapped. Details of the mapping procedure are described by Richardson (2003).

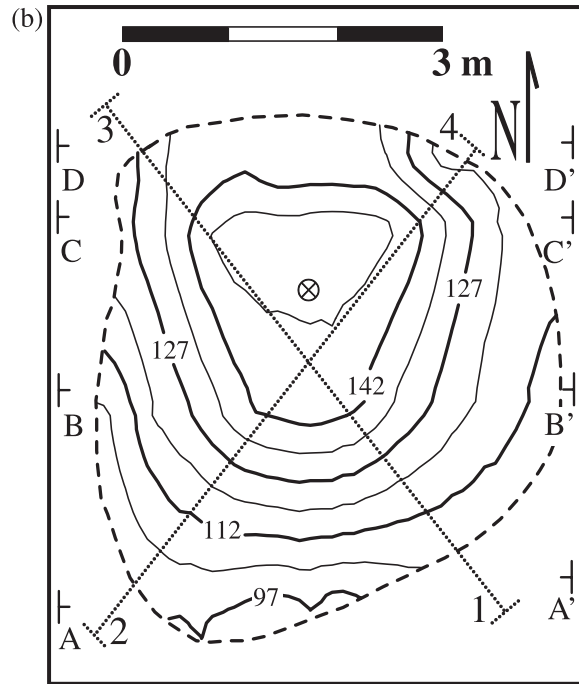
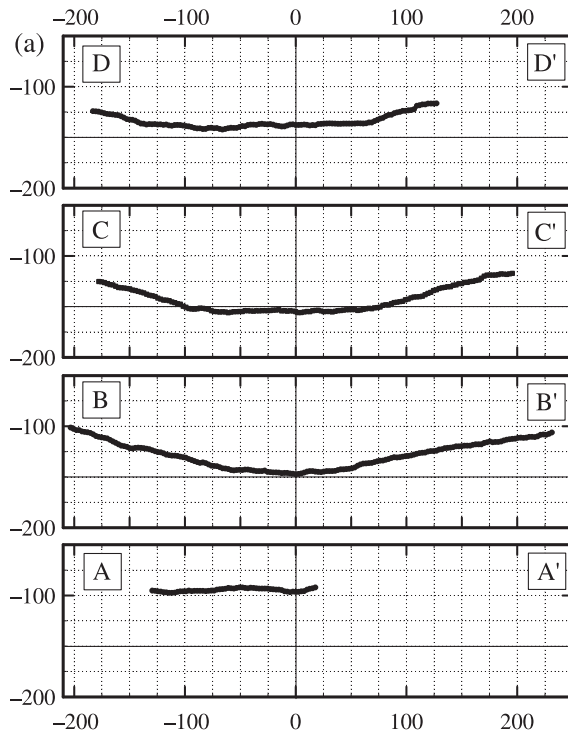
A total of 67 m of fracture trace was mapped and the information was digitized by recording the vertical aperture, altitude, and percentage of each sand color every 2.5 cm. The resulting dataset includes a total of 2685 points along the exposure. Contour maps were generated using kriging with a linear variogram. The data were much more closely spaced along the trench faces than perpendicular to them, and this created a bias toward correlations that were parallel to the trench faces. Anisotropic variograms were used in some cases to accentuate the correlation between opposing trench faces, which produced maps that were more consistent with manual interpretations. Isotropic variograms were used, however, to create the maps shown here to avoid using an arbitrary anisotropy.

Observations

Monitoring during fracture creation showed pressure signals that increased sharply to approximately 300 kPa and then decreased with time (Fig. 2). Sharp pressure drops accompanied periodic sampling of the injected slurry, and minor fluctuations in pressure were common. The ground surface was displaced upward, creating broad domes of 1–2 cm amplitude that roughly coincided with the extents of the fractures.

Three fractures overlapped in plan view, but they were at different elevations and none of them intersected (Fig. 1). As a result, we expect that the forms represent isolated fractures

Fig. 3. (a) Serial cross sections and (b) map of centimetres below datum to fracture H. The end points of cross sections in (a) are indicated on the map in (b) along with end points of cross sections in Fig. 10 labeled 1, 2, 3, and 4.



that were not influenced by preexisting neighboring hydraulic fractures.

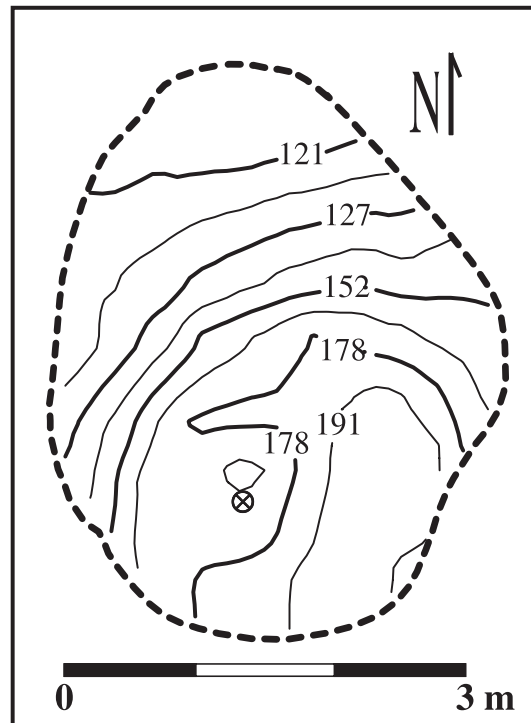
Form

The fractures resembled irregular saucers with lateral extents of 4.5–7.0 m. They were roughly flat-lying or gently rippled in the vicinity of the borehole (Figs. 3, 4), but they curved upward with increasing distance from the borehole. The flat-lying region extended roughly 1.5 m from the borehole, a distance equal to the depth of the fracture. It was flanked by a region whose dip was 10° to 20°, which extended as far as 5.5 m from the borehole (Fig. 4). The gently dipping region wrapped around three sides of fracture I (Fig. 4), but it only occurred on two sides of fracture H (Fig. 3). One side of each of the other two fractures was not excavated, so the complete symmetry of those fractures is unknown.

The fracture in the vicinity of the borehole (i.e., fracture I) curved downward to create a shallow, trough-like structure (Fig. 4), and similar features were associated with fractures G and F. The bottoms of the troughs commonly were 0.3 m below the notch, but one part of fracture F extended to 0.7 m below the notch. Saprolite was within 0.5 m below all of the regions where fractures propagated downward, but the saprolite contact was deeper (more than 0.6 m) below fracture H, which propagated horizontally and upward (Fig. 3). Field evidence suggests the downward propagation was related to proximity of underlying saprolite.

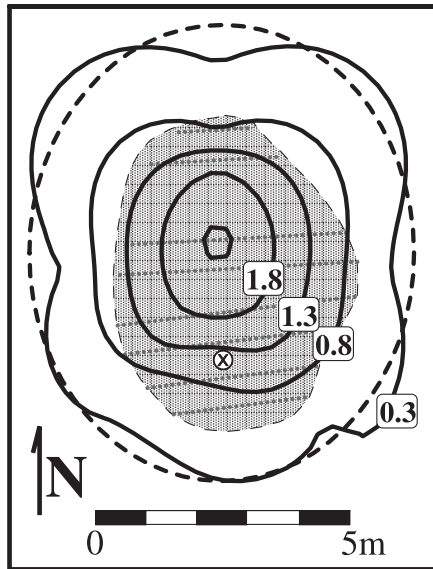
All the fractures curved upward, and they did so as a series of steps over scales of a few centimetres to a few tens of centimetres (Richardson 2003, his Fig. 4.1-4). Typically, a fracture would curve upward and then flatten. The rough appearance of the fracture traces in Fig. 3 results from the small steps, and some larger steps are evident on the section.

Fig. 4. Structural contours on fracture I in centimetres below datum at the ground surface. ⊗, injection casing.



All the fractures were slightly elongate and asymmetric. The degree of elongation was characterized by aspect ratios that ranged from 1.1:1 to 1.4:1, with an average value of 1.2:1. For comparison, the aspect ratios of nearly 100 fractures created in a variety of geologic settings other than

Fig. 5. Uplift contours (solid line) over fracture I in centimetres. The extent of sand is stippled. The ellipse (broken line) is used to represent uplift. ⊗, injection casing.



saprolite ranged from 1.0:1 to 1.4:1, with an average value of 1.2:1 (Murdoch and Slack 2002). Asymmetry was characterized by borehole and displacement eccentricities. These values were determined by fitting an ellipse to measurements of uplift (Fig. 4). *Borehole eccentricity* is the distance from the center of the ellipse to the borehole scaled to the length of the major axis of the ellipse. Borehole eccentricity ranged from 0.12 to 0.21, and the average value was 0.17. Murdoch and Slack (2002) reported an average value of 0.14 for borehole eccentricity. *Displacement eccentricity* is the distance from the injection casing to the point of maximum uplift scaled to the length of the major axis. Displacement eccentricities ranged from 0.12 to 0.27, with an average of 0.18. For comparison, the average displacement eccentricity of the fractures summarized by Murdoch and Slack is 0.14. The fractures created for this work are remarkably similar to many others reviewed by Murdoch and Slack, and they are consistent with other field characterizations described by Frere and Baker (1995) and Wong and Alfaro (2001).

Uplift and extent of the fracture

Uplift measurements resemble elliptical domes, and the uplift contours were evaluated as a method for estimating the extent of the underlying fracture. Careful excavation revealed a parting that extended up to 0.15 m beyond the leading edge of the sand in most exposures. Presumably, the parting was open when the hydraulic fracture was pressurized. Evidence for an open fracture farther than approximately 0.15 m from the edge of sand is absent, however, despite careful inspection in these areas. The lateral extent of the sand-filled portion of the fracture is therefore assumed to represent the overall lateral extent of the open fracture.

The uplifted domes were offset from the injection casing in the same direction, and nearly the same distance, as the center of the sand was offset from the casing. The extent of sand was always within the uplifted area, and the region containing sand was typically contained within the 7 mm up-

Fig. 6. Cross sections of sand thickness (○) and uplift (◇) along the major axis of fracture G. Third-order polynomial fits for sand thickness (solid line) and uplift (broken line).

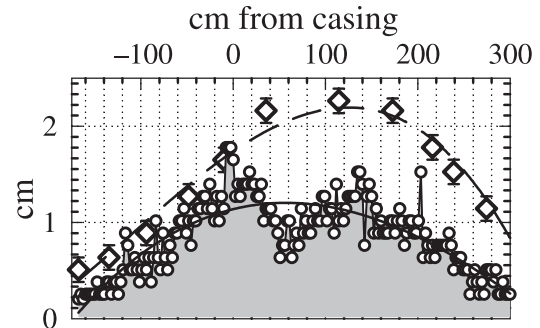
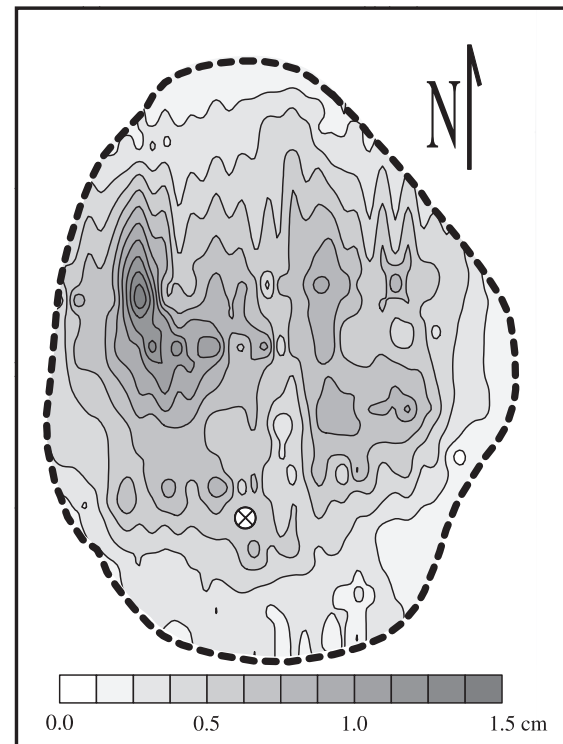


Fig. 7. Distribution of sand thickness in fracture I. ⊗, injection casing.



lift contour (Fig. 5). The extent of sand varied within the uplifted region, however, and the extent was contained locally within uplift contours as small as 2 mm to as large as 17 mm.

Sand thickness

In general, sand thickened from the edge to the center of a fracture, but considerable variations occurred. The sand thickness varied by roughly 0.3–0.5 of the average thickness over lateral distances of a few centimetres to 0.5 m (Fig. 6). This amount of variation is typical of all the profiles. Some of the changes in thickness appear to be related to steps in the fracture, with the sand thickening on the flat part of the step and thinning on the riser.

The serial sections in fracture I allowed the sand thickness variations to be interpolated over the fracture. This shows variations in sand thickness as bands originating at the casing and extending along the long axis of the fracture (Fig. 7). A

band of unusually thick sand extended to the north-northeast of the borehole, whereas an atypically thin band occurred along the long axis slightly east of the borehole (Fig. 7).

The use of uplift pattern as a predictor of sand distribution was evaluated by comparing the magnitude of uplift to the average sand thickness, obtained by fitting a third-order polynomial to the thickness data (Fig. 7). The ratio of sand thickness to uplift typically ranged from 0.30 to 0.45 over most of the fractures, although locally this ratio ranged from 0.15 to 0.70 (Richardson 2003, his Figs. 4.1-13, 4.1-14, 4.2-8, 4.3-5, and 4.4-5). For comparison, the sand loading (ratio of the bulk volume of settled sand to the total volume) in the slurry was approximately 0.3 for all the fractures. The sand loading would also be the ratio of the sand thickness to the total inflated thickness of the fracture. The results show that typical values of the ratio of average sand thickness to uplift are roughly equal to or approximately 1.5 that of the sand loading.

These observations suggest that measurements of uplift and sand loading could have been used to estimate a lower bound of the *average* sand thickness in this particular field test. Sand is generally thicker than this estimate and highly variable (Figs. 6, 7), however, so a sample obtained from any particular location may vary considerably (by at least ± 0.5) from the estimated average.

In other applications where the fracture is deep relative to its maximum extent, the uplift may be considerably less than the aperture. The results shown here suggest that predictions of aperture distribution (instead of the uplift) could have been used along with the sand loading to estimate the average sand thickness.

Color distribution

The distribution of different colors of sand in the fracture was estimated by visual inspection in the field, and it was determined by point counts of samples of slurry taken at regular intervals during the fracture injection. The sand-color distribution data derived from point measurements on the cross sections were interpolated and plotted as individual maps (Fig. 8). These data show that the red sand, which was injected first, occurred within approximately 2 m of the injection casing and was essentially absent beyond this distance. The red sand south of the injection casing formed north-south-trending ridges (Figs. 7, 8). White sand occurred throughout most of the fracture, but was absent from the northern leading edge (Fig. 8). The greatest percentages of white sand occurred in the eastern and southeastern portions of the fracture. The lowest values were in a north-south-trending band extending from the injection casing where white sand was as sparse as 20%. Blue sand, the last to be injected, occurred north of the injection casing (Fig. 8). The highest percentages of blue sand occurred in a north-south-trending band approximately 0.6 m wide extending north from the injection casing, the same band where the fraction of white sand was lowest. Interestingly, the sand was relatively thin along this band, e.g., compare Figs. 7 and 8. The band of blue sand extended from the injection casing northward along the major axis and then fanned out along the northern edge of the fracture.

Another band of blue sand trended roughly N20°W from the injection casing (Fig. 8). This band also was associated

with a region where the white sand was relatively sparse, and it too extended from the casing to fan out at the leading edge. The N20°W band contained mixtures of blue and white sand, along with sand that was totally blue. In contrast, the north-trending band contained only blue sand, so it was injected after the N20°W band.

Many cross-sectional exposures revealed structures of younger sand embedded in older sand, as indicated by contrasts in sand color. The contact between the two different colors of sand was typically sharp, and it was always concave toward the younger sand. In some exposures, the contact curved downward from the upper surface of the fracture, flattened out, and curved back up to the upper surface. This produced a structure that resembled a deposit of channel sand viewed in cross section perpendicular to the flow direction. In other exposures, the contact curved downward from the upper wall and intersected the lower wall, and this contact was typically mirrored by another one nearby. These exposures resembled the channel-like pathways, but they were thicker and wider. Similar structures were observed where granular graphite was injected into a sand-filled fracture; the channel-like pathways filled with graphite displaced the earlier sand (Roulier et al. 2000) (Figs. 5, 6). Related features have also been observed in laboratory experiments (Lowe and Huitt 1966).

The channel structures were clearly cross-sectional exposures of the bands of colored sand described previously. These structures were shaped like channels in cross section, they were elongate features that branch in the direction of flow, and they cut sand that was deposited previously.

Surfaces of hydraulic fractures

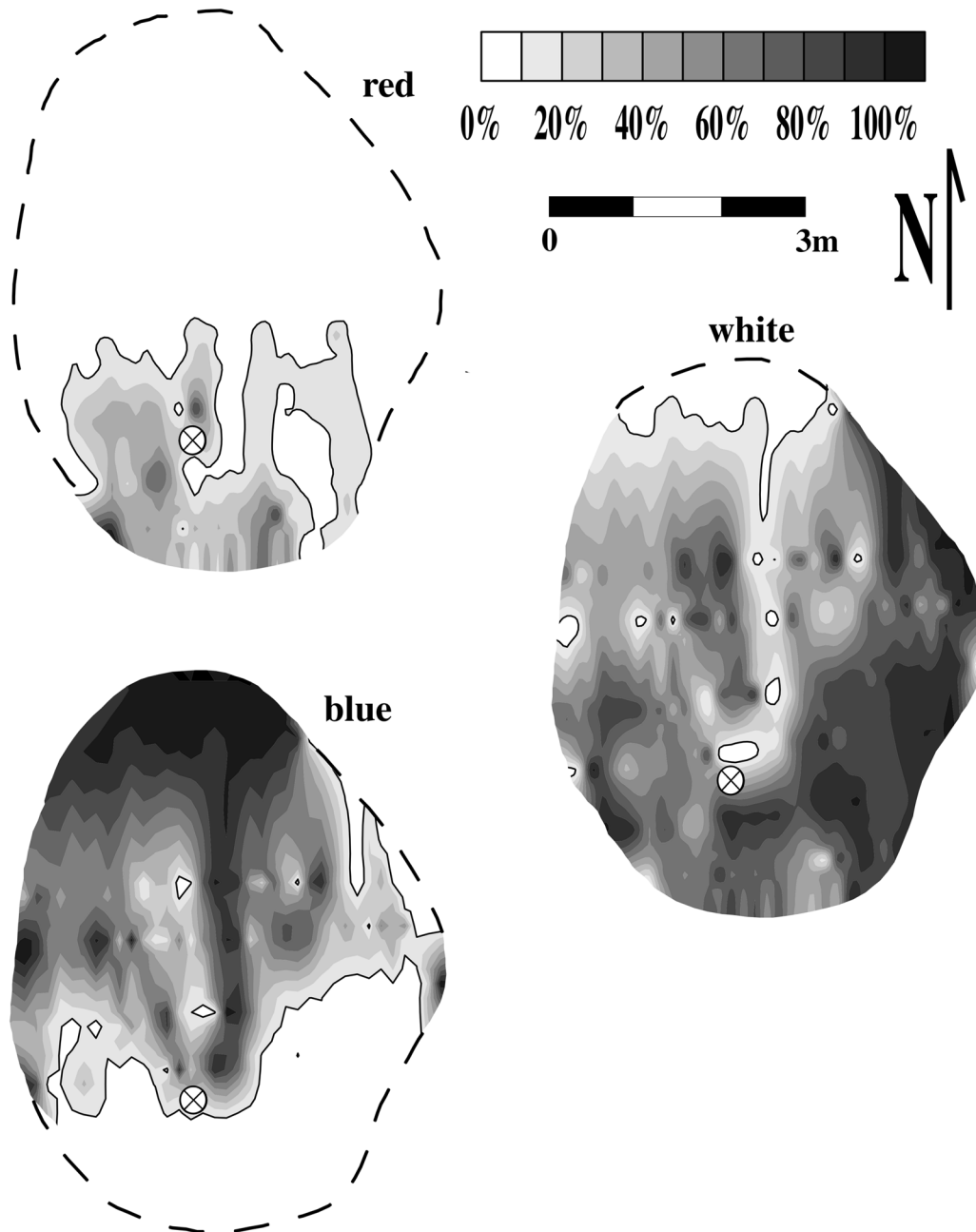
Three areas were exposed by carefully removing the overburden to reveal the upper surface of the sand. The distribution of sand colors and features on the fracture surfaces in these areas were mapped in plan view. Patterns formed by the sand colors on the top of the fracture were delineated with pins pushed into the underlying material. Then the loose sand was removed with a vacuum cleaner. Sand grains sticking to the bottom surface of the fracture remained in place, and the patterns formed by these different colors were mapped using the pins as reference points. Then the sand was completely removed to reveal a series of steps on the fracture surface. Locations of colored bands, strips of color on the lower surface, and the steps were included in the map (Fig. 9).

The upper surface of the northwestern exposure was characterized by bands of blue sand separated by white sand (Fig. 9). Both regions actually consisted of mixtures of colors, but the regions labeled as blue sand were dominantly that color, with subordinate amounts of white sand. The regions labeled as white sand also contained minor blue sand.

The bands of blue sand trended roughly east-west and were 15–30 cm wide (Fig. 9). The bands were well defined, and they split with increasing distance from the injection casing. Two blue bands occurred on the eastern end of the northwestern exposure. The southernmost band split into five bands across the exposure (Fig. 9). The northernmost band appeared to split into two bands, but the ends of these bands were removed during excavation, so the full extent of the bifurcation was unknown.

The lower surface of the fracture was marked with a dendritic pattern of narrow strips of blue sand (Fig. 9), which

Fig. 8. Maps of sand color percentage data interpolated from cross sections of fracture I.



were revealed after approximately 4 mm of the overlying sand was removed. The strips of blue sand were 3–10 cm wide and formed a branching pattern that corresponded to the axes of the wider blue bands. Several of the blue strips appeared to have split within a blue band near the western edge of the fracture (Fig. 9). Orientations of both blue strips and blue bands appeared to be perpendicular to the leading edge of the fracture in the vicinity.

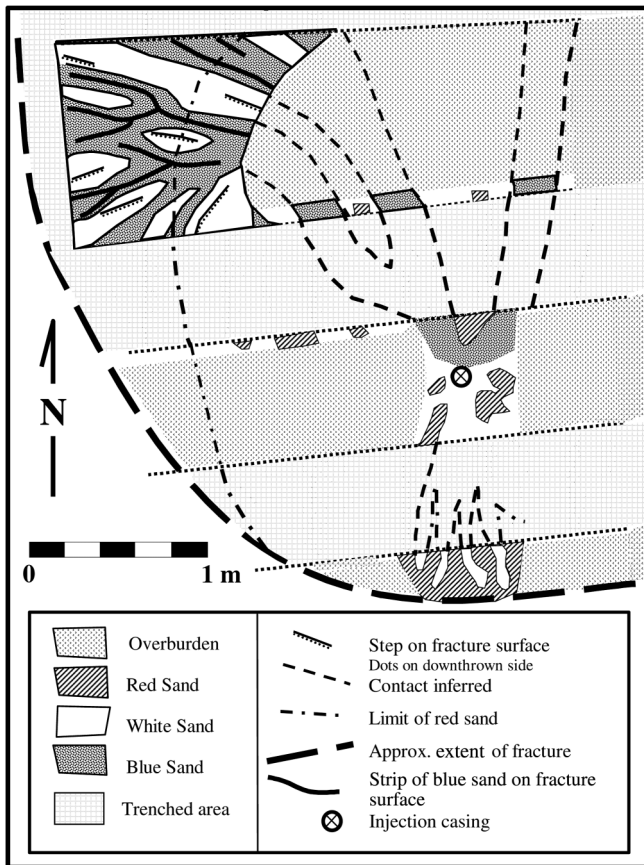
The blue bands appeared to be channel pathways, although none of them could be examined in cross section. The blue strips on the lower surface of the fracture appeared to be deposited where the thickest part of the channel spanned the entire fracture.

The lower surface of the fracture was formed from massive sandy, clayey silt typical of the B soil horizon. The surface

was slightly irregular, but there were several steps where the elevation changed abruptly by 2–5 cm. The steps formed linear features from 10 cm to more than 30 cm long. Six steps were clearly evident on the fracture surface, and they all occurred in areas of white sand between the bands of blue sand. They all were roughly parallel to the blue bands and strips in their vicinity. As a result, the orientation of the steps radiated from west-northwest to southwest, following the orientation of the bands. The downthrown sides of the steps were also consistent; the downthrown side was always to the south (Fig. 9).

A region to the south of the injection casing was also exposed by excavation, and the pattern here resembled that of the northwestern area but with some important differences. This region was approximately 0.2 m² and revealed the lead-

Fig. 9. Distribution of sand colors and features associated with fracture I.



ing edge of the fracture. Sand in this region was several grains thick, and most of the sand was red. Four bands of white sand extended from the trench face southward and terminated slightly north of the leading edge (Fig. 9). The bands were 3–6 cm wide, and their exposed length ranged from 10 to 30 cm. Their leading edges were rounded in plan.

One observation that may be significant is that patches of red sand in the vicinity of the casing clearly spanned the entire thickness of the fracture. Red sand was injected first, and the fracture aperture near the casing probably was roughly half of the final aperture when the last of the red sand was injected. The red sand filled the entire fracture, however, so it appeared that the thickness of the red sand increased to fill the growing fracture.

Simulating fracture form

A numerical model describing the propagation of a hydraulic fracture beneath an interface was created by modifying a code called Franc2d (Wawrzynek and Ingraffea 1994), which is widely used to simulate fractures in mechanical structures. Modifications were made in Franc2d so that it would (i) include loading due to transient fluid flow, and (ii) automatically adjust boundary conditions to ensure that the stress intensity equals the fracture toughness during propagation (details of the code modifications are outlined by Tan 2003). These modifications are similar to those of other numerical methods used to simulate hydraulic fracturing (Nilson and

Griffiths 1983; Valko and Economides 1995; Murdoch and Germanovich 2006). However, unlike conventional methods designed to analyze planar, vertical cracks, our modification of Franc2d can predict the geometry of axisymmetric fractures that curve upward because of mechanical interactions with the ground surface, buoyancy effects, or other related processes. The algorithms used to predict the trajectory of a propagating fracture in Franc2d assume the fracture propagates in the direction of the maximum circumferential stress at the crack tip (Ingraffea 1987), an approach that is widely used to predict propagation paths in linear elastic materials.

The model was set up to include conditions representing the field site. Body forces from the weight of the soil were included, along with a horizontal residual stress of 72 kPa (the average from field measurements). The formation was initially assumed to be uniform, and parameters were adjusted to match observed data for injection pressure and uplift of fracture H, which resulted in an elastic modulus of $E = 37$ MPa, Poisson's ratio of 0.4, and fracture toughness of $K_{Ic} = 0.3$ MPa·m^{1/2}.

Injection pressure and form

The model predicts that the injection pressure should decrease as a function of time (Fig. 2). The observed pressure log is more erratic than the predicted log because the model lacked some details, like opening a valve to sample the slurry, which caused irregularities in the observed log. Nevertheless, the predicted log resembles observed pressures remarkably well (Fig. 2).

The model assumes axial symmetry, but all the fractures were asymmetric about the injection point. To address this discrepancy, cross sections were made along lines trending northeast–southwest and northwest–southeast that intersect at the center of fracture H (Fig. 3), and these data were compared with the predicted results.

The simulated cross section resembles two of the observed traces and occurs within the envelope created by the four sections (Fig. 10). Two other traces on the southwest and southeast sides of the casing climbed more quickly than the simulation predicts. Interestingly, even where the model failed to predict the correct location of the fracture trace, it did a fairly good job of predicting the dip. The simulated fracture dips approximately 16° at the periphery, whereas the dip of the real fracture was in the range of 15°–20°.

The results of the simulation were also compared with observed uplift and distribution of sand (Fig. 11). The extent of sand was somewhat variable and ranged over a radial distance (r) of 2.0–2.5 m from the center of the fracture, and the predicted extent of the fracture occurred within this range (Fig. 11). The predicted maximum uplift was the same as the observed uplift, but the distributions of uplift were somewhat different. The model predicted uplift that was roughly uniform out to approximately $r = 1$ m and then decreased to zero slightly past $r = 2$ m. The observations indicated that uplift tapered fairly gradually over 3 m or more.

Downward propagation

Three of the hydraulic fractures propagated downward slightly and then curved upward, and we expected this peculiar form may have been related to the presence of saprolite beneath these fractures. These expectations were tested by

Fig. 10. Predicted (thick line) and observed (symbols) fracture traces in cross section, fracture H. Observed data from sections located in Fig. 3. Δ and ∇ , sections 1 and 2; \square , section 3; \circ , section 4.

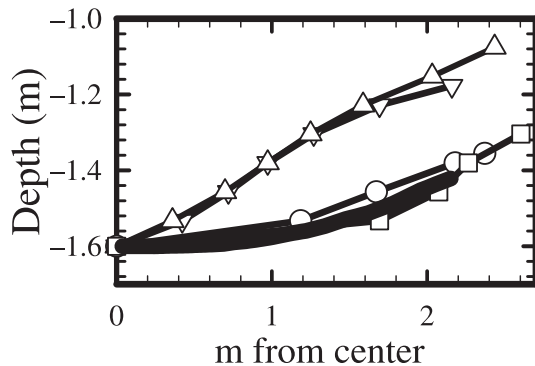
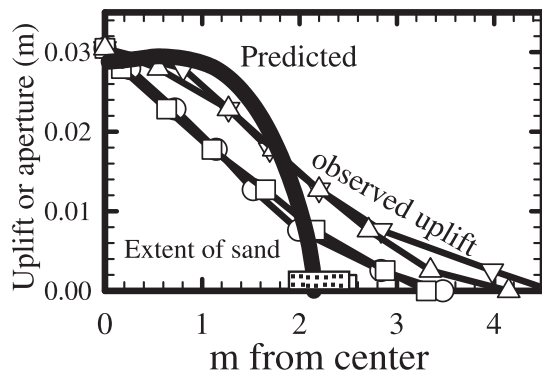


Fig. 11. Fracture aperture profile from simulation (thick line) and field measurements of uplift (symbols) and the radial extent of sand from a central point (stippled) in fracture H. Δ and ∇ , sections 1 and 2 in Fig. 3; \square , section 3 in Fig. 3; \circ , section 4 in Fig. 3.

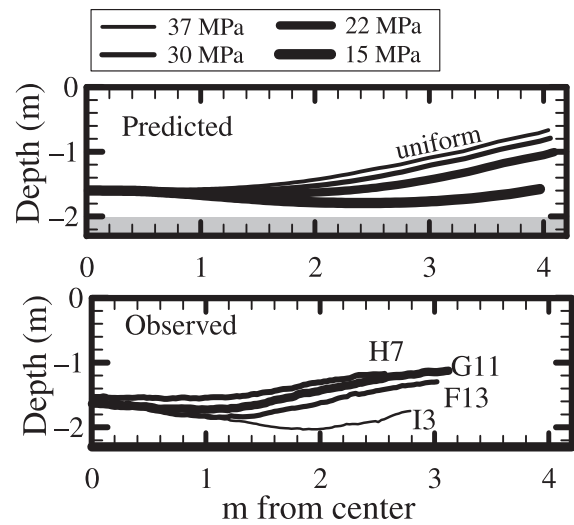


conducting several simulations where the saprolite was represented as an underlying layer with a different elastic modulus. We were unable to obtain direct measurements of the modulus of the saprolite, but we assumed it was softer than that of the overlying B horizon and several values of E were evaluated (Fig. 12).

The presence of the underlying soft layer caused the simulated fracture to curve downward and then back upward toward the ground surface (Fig. 12). Increasing the contrast in modulus or decreasing the distance to the underlying interface increased the downward curvature. Fracture traces observed in the field were variable, but they include the forms predicted theoretically with an underlying soft layer (Fig. 12).

The fracture curves because the low-modulus layer affects the stresses at the crack tip. The side of the fracture nearest the low-modulus layer deflects toward the layer, and this produces tension on that side of the tip, causing the fracture to curve. The magnitude of this effect is small when the radial length of the fracture is shorter than the distance to the low-modulus layer, but the effect increases as the fracture lengthens. This causes the incipient fracture to first curve downward toward the nearby, soft layer beneath it, but the growing fracture becomes increasingly influenced by the overlying free surface, which itself behaves like a contact with a

Fig. 12. Predicted fracture traces in a layer of elastic modulus $E = 37$ MPa underlain by a softer layer (shaded) with modulus given in legend. Observed fracture traces along trench faces (indicated by fracture letter and trench number).



layer of extremely low modulus. Once the radial length of the fracture exceeds the depth, the influence of the overlying free surface dominates that of the low-modulus layer and the fracture curves upward.

Discussion

Details of the form and sand distribution in the fractures created for this investigation are more complicated than we initially expected, but many of them are consistent with existing theories or observations from laboratory studies. The field evidence suggests that sand transport is characterized by the following observations: (i) the earliest sand to be injected was deposited closest to the injection casing, and the last sand to be injected was at the leading edge of the fracture; (ii) sand migrated in localized, channel-like pathways that displaced sand injected earlier; (iii) major channel-like pathways occurred near the injection casing and split into many paths as they approached the leading edge of the fracture; (iv) the locations of individual sand pathways were related to the locations of features, such as steps and cusps on the fracture surface, that result from the mechanical processes of fracture propagation; and (v) the thickness of sand was related to the timing of injection: sand injected early thickened during subsequent injection, whereas the last sand to be injected was thinner than the earlier material.

Sand transport in horizontal hydraulic fractures has been studied in the laboratory by injecting various slurry concentrations in transparent, horizontal slots and then photographing the resulting patterns (Kern et al. 1959; Wahl and Campbell 1963; Lowe and Huitt 1966). These studies showed that sand is transported when the concentration is low and the velocity is high, whereas it can be deposited when the concentration increases or the velocity decreases. They recognized that sand can be deposited in some regions of the experimental apparatus and remain mobile in others. Interestingly, the pattern of mobile sand in the laboratory experiments seems to be strikingly similar to the distribution of sand in the field tests

conducted here. Lowe and Huitt (1966, p. 756) state the following: “The slurry then moved through the deposit in fingers. Growth of the fingers was much like the growth of the delta area of a river... After the dunes and channels became stable, particles moved only through the channels. Because of this, it was assumed that essentially all of the fluid flowed through the channels... The channels are made up of many branches rather than extending outward in a straight line.” Those same descriptions and geologic analogies are relevant to the field exposures created during this investigation.

The laboratory experiments showed that sand slurry moves through discrete channels that cut through relatively immobile sand banks (the “dunes” from Lowe and Huitt 1966). The descriptions presented here confirm that basic mechanism at the field scale, and additional support is given by Roulier et al. (2000) (Figs. 5, 6). The field conditions from this study differ from the laboratory experiments in several important ways, however, and this resulted in several additional conclusions. Lowe and Huitt (1966) (Fig. 11) inferred that channels would be absent from the vicinity of the well because the flow velocity would be too high for sand to be deposited and channels to form. Instead, they inferred (their experiments used linear flow, so the effects of decreasing velocity in radial flow could only be inferred) that the sand would be transported as a continuously moving sheet in the vicinity of the wellbore. Our work shows that channels of several generations occur in the vicinity of the well (Figs. 8, 9). This is significant because the distribution of sand adjacent to the well plays an important role in well performance.

The walls of the apparatus used in laboratory experiments (Wahl and Campbell 1963; Lowe and Huitt 1966) were smooth. It is noteworthy that localized channels developed in those tests even though the fracture walls in the experiments lacked preferential paths. The walls of real fractures are rough, and the pattern of roughness is at least partly a result of the propagation process. It is generally recognized that small fracture lobes grow and coalesce at the leading edges of propagating dilational fractures, including hydraulic fractures (Pollard et al. 1975). Isolated lobes have been recognized at the leading edge of some fractures. In other cases, cusps, steps, hackle marks, or offsets on fracture surfaces are interpreted as features created where mechanical lobes coalesce (Pollard 1973; Pollard et al. 1975, 1982). This process produces steps and offsets that inevitably create paths along a fracture that gape open wider than those in neighboring regions. The field observations for this work indicate that the sand channels are preferentially located along these wider paths (the regions between the steps in Fig. 9).

It is generally recognized that there is a coupling between fluid flow and normal displacement in hydraulic fractures, but most theoretical analyses only consider how this coupling occurs in a smooth-walled fracture. The results of this work confirm that there is a basic coupling between the fracturing process and fluid flow, but the details differ from the basic assumptions. It appears that mechanical responses within the fracture process zone that result in lobe creation and coalescence create subtle variations in aperture that localize fluid flow and sand transport within the fracture. Similarly, localized fluid flow is expected to result in a variable fluid pressure distribution that will affect lobe creation. This detailed interaction seems to be beyond the scope of

current theoretical analyses (e.g., Murdoch and Germanovich 2006).

Observations from fracture I can be interpreted based on the processes outlined previously. Maps of sand distribution (Figs. 8, 9) show at least four major pathways that split as they approached the leading edge. The first one of the four to be emplaced was filled with white sand, and it displaced red sand to the south of the injection casing. The fan structure (similar to the “delta” of Lowe and Huitt 1966) that was observed in the most detail was filled with blue sand and occurred to the northwest of the injection casing (Fig. 9). The last channel that was active extended northward from the casing and terminated at the northernmost edge. The last active pathway is only partly shown in Fig. 9, but it is well represented by the distribution of blue sand (Fig. 8) and by a band of unusually thin sand in Fig. 7. The four bands in Fig. 9 are probably only a few of the pathways that transported sand in fracture I.

Sand apparently can thicken after it has been deposited and is relatively immobile. This is best illustrated by the red sand that spans the entire thickness of the fracture near the injection casing where the sand is two to three times the thickness that would be predicted by sand loading of the red sand slurry. Elsewhere, white sand appears to have been pushed into the lateral edges of fracture lobes by channels of blue sand. It seems that sand moves large distances through localized pathways, but it can move small distances and thicken after it has been deposited. This is further supported by the atypically thin sand in the last channel to be active, the one filled with blue sand (Fig. 7).

Predicting fracture form

Fractures created during this work curved out of their original plane. All of the fractures curved upward, and a few propagated downward before curving up. The general form created by a hydraulic fracture that gently curves upward characterizes the fractures created for this work, and it appears to be typical of many shallow applications described previously (Murdoch et al. 1994; Murdoch 1991, 1995; Frere and Baker 1995; Wong and Alfaro 2001; Murdoch and Slack 2002).

The upward-curving, saucer-like form can be predicted using a two-dimensional theoretical model that simulates the propagation path of a hydraulic fracture using principles of fracture mechanics. The model also predicts a pressure log that resembles observed pressures. This appears to be the first validation of a theoretical model that is capable of predicting the form of a curving hydraulic fracture at shallow depths. The model confirms expectations (e.g., Murdoch 1995; Wong and Alfaro 2001) that residual stress representing over-consolidated conditions is required to create gently dipping hydraulic fractures at shallow depths — simulated fractures curved upward to dip steeply when the residual stress was absent (Tan 2003).

Gentle troughs created by downward propagation of the fracture surrounding the injection casing of fractures F, G, and I have to our knowledge never been described in other exposures. The theoretical model predicts that a hydraulic fracture should propagate downward toward an underlying interface with softer material, and it predicts fracture forms that resemble the peculiar forms observed in the field.

Downward propagation resulted in changes in form that were small relative to those of the overall fracture, but those changes could have significant consequences. Prior to this study, we assumed that fractures were horizontal or curved upward because downward propagation had never been described and it seemed unlikely to occur under idealized mechanical conditions. As a result, efforts to locate fractures by core sampling were typically terminated when the sampler reached the depth of the notch. Fractures were not detected in several locations using this procedure, and it now appears likely that they were missed because slight downward propagation caused the fracture to propagate deeper than expected.

The theoretical model developed for this work appears to be capable of predicting forms typical of many shallow hydraulic fractures, and it can predict an atypical form that results from special geologic conditions at the field site. These results suggest that linear elastic fracture mechanics (LEFM) is a viable approach for predicting the forms of curving hydraulic fractures in shallow cohesive soils. This builds on the conclusions of Murdoch (1991, 1993a, 1993b, 1993c) and Harison et al. (1994), who showed that LEFM can explain laboratory observations. It also provides a tenable method for predicting how subsurface conditions affect the dips of hydraulic fractures. This is important because dips can range from flat-lying to vertical, and the dip plays an important role in how a hydraulic fracture can be used. Although these results are encouraging, it is important to recognize that the model has only been demonstrated at a single site, and considerably more effort is required before the capabilities and limitations of this approach can be fully evaluated. For example, recent work by Wu (2005) suggests that the LEFM approach may be inappropriate for fractures in cohesionless material.

Conclusions

Hydraulic fractures created at a depth of 1.5 m in residual soil resemble asymmetric saucers from 4.5 to 7.0 m in maximum dimension (Figs. 3, 4). The fractures were filled with sand up to 2 cm thick, and sand was generally thinner on the edge and thicker in the middle of a fracture (Fig. 6). The general sand distribution over the scale of the fracture could be represented by a third-order polynomial, but at smaller scales the thickness was highly variable (Fig. 6) and typically ranged between ± 0.3 and 0.5 of the thickness defined by the polynomial over distances of a few centimetres to a few tens of centimetres (Fig. 6). Systematic variations in thickness also occurred at larger scales, with bands of atypically thick or thin sand extending from the borehole to the leading edge of the fracture (Fig. 7).

Sand moved through localized pathways as it filled the hydraulic fractures created for this work (Fig. 9). The pathways resembled stream channels in cross section and extended from the injection casing to the leading edge, where they fanned out to distribute sand through a branching network (Figs. 8, 9). This caused sand to move rapidly to the leading edge of a fracture, instead of spreading slowly from the injection casing as would be expected if the flowing fluid uniformly filled the entire fracture. At least four such channels could be identified in one fracture, and they became inactive at different times during propagation (Fig. 8).

Channel structures occurred between offsets and steps on the fracture surface formed where fracture lobes coalesced (Fig. 9). This seems to represent an interaction between the mechanical breaking of the fracture and the development of a branching network of channels carrying slurry through the fracture.

The distribution of sand could be crudely predicted by estimating the aperture of the pressurized fracture. The extent of sand was approximately defined by the 7 mm contour of aperture (or uplift) during this work (Fig. 5). The ratio of the average thickness of sand to the uplift is roughly 0.4, and this is somewhat greater than that of the average sand loading in the slurry (approximately 0.3) (Richardson 2003). This suggests that it might be feasible to predict the gross sand distribution as the product of sand loading and inflated aperture; however, interactions between the flow of sand-laden slurry and the mechanical breaking of the fracture appear to have caused the distribution of sand to vary markedly throughout the fracture (Fig. 7). Advances in predicting sand distribution appear to require consideration of these interactions.

The forms of hydraulic fractures created during this work (Figs. 10, 11), including some peculiar forms (Fig. 12), can be predicted using a two-dimensional model based on linear elastic fracture mechanics coupled with a fluid mechanics analysis. This approach shows promise as a method for predicting the forms and general distribution of solids by hydraulic fracturing. Detailed predictions of the transport of sand within a fracture appear to require consideration of wall roughness developed during propagation, however.

Acknowledgements

We appreciate support from the National Science Foundation under grants EAR 9876124 and EAR 0001146. Many thanks to Bill Slack, Leonid Germanovich, Bruce Carter, Wash Wawrzynek, Ron Andrus, Billy Camp, Monty Busbee, Todd Lackey, and Doug Knight for their insights and assistance.

References

- Baker, E., and Leach, B. 1995. Soil fracturing cracks soil remediation barriers. *Environmental Solutions*, **8**: 26–27.
- Bradner, G., and Murdoch, L.C. 2005. Effects of skin and hydraulic fractures on the performance of an SVE well. *Journal of Contaminant Hydrology*, **77**: 271–297.
- Frere, J.M., and Baker, J.E. 1995. Use of soil fracturing to enhance soil vapor extraction, a case study. *In Proceedings of the ACS Specialty Symposium on Emerging Technologies in Hazardous Waste Management VII*, Atlanta, Ga., 17–20 September 1995. American Chemical Society (ACS), Washington, D.C. pp. 17–20.
- Gidley, J.L., Holditch, S.A., Nierode, D.E., and Veatch, R.W. 1989. Recent advances in hydraulic fracturing. *Society of Petroleum Engineers Monograph* 12. 452 pp.
- Harison, J.A., Hardin, B.O., and Mahboub, K. 1994. Fracture toughness of compacted cohesive soils using a ring test. *Journal of Geotechnical Engineering*, ASCE, **120**: 872–891.
- Howard, G.C., and Fast, C.R. 1970. Hydraulic fracturing. *Society of Petroleum Engineers, American Institute of Mining, Metallurgical and Petroleum Engineers (AIME)*, New York. 198 pp.

- Ingraffea, A.R. 1987. Theory of crack initiation and propagation in rock. *In Fracture mechanics of rock*. Edited by B.K. Atkinson. Academic Press Inc. (London) Ltd., London, UK. pp. 71–110.
- Kern, L.R., Perkins, T.K., and Wyant, R.E. 1959. The mechanics of sand movement in fracturing. *Transactions of the American Institute of Mining, Metallurgical and Petroleum Engineers*, **216**: 403–405.
- Lowe, D.K., and Huitt, J.L. 1966. Propping agent transport in horizontal fractures. *Journal of Petroleum Technology*, **18**: 753–763.
- Malin, S.C. 2005. In situ stress determination in unsaturated soils using hydraulic fractures. M.Sc. thesis, Clemson University, Clemson, S.C. 148 pp.
- Murdoch, L.C. 1991. The hydraulic fracturing of soil. Ph.D. dissertation, University of Cincinnati, Cincinnati, Ohio. 206 pp.
- Murdoch, L.C. 1993a. Hydraulic fracturing of soil during laboratory experiments: methods and observations. *Géotechnique*, **43**(2): 255–265.
- Murdoch, L.C. 1993b. Hydraulic fracturing of soil during laboratory experiments: propagation. *Géotechnique*, **43**(2): 266–276.
- Murdoch, L.C. 1993c. Hydraulic fracturing of soil during laboratory experiments: theoretical analysis. *Géotechnique*, **43**(2): 277–287.
- Murdoch, L.C. 1995. Forms of hydraulic fractures created during a field test in overconsolidated glacial drift. *Quarterly Journal of Engineering Geology*, **28**: 23–35.
- Murdoch, L.C. 2000. Remediation of organic chemicals in the vadose zone. *In Vadose zone science and technology solutions*. Edited by B.B. Looney and R.W. Falta. Battelle Press, Columbus, Ohio. Chap. 7, pp. 948–1247.
- Murdoch, L.C. 2002. Mechanical analysis of an idealized hydraulic fracture at shallow depths. *Journal of Geoenvironmental and Geotechnical Engineering, ASCE*, **128**: 488–495.
- Murdoch, L.C., and Chen, J.-L. 1997. Effects of conductive fractures during in situ electroosmosis. *Journal of Hazardous Materials*, **55**: 239–262.
- Murdoch, L.C., and Germanovich, L. 2006. Analysis of a deformable fracture in permeable material. *International Journal for Numerical and Analytical Methods in Geomechanics*, **30**: 529–561.
- Murdoch, L.C., and Slack, W. 2002. Forms of hydraulic fractures in shallow fine-grained formations. *Journal of Geotechnical and Geoenvironmental Engineering, ASCE*, **128**: 479–487.
- Murdoch, L.C., Wilson, D., Savage, K., Slack, W., and Uber, J. 1994. Alternative methods for fluid delivery and recovery. Report USEPA/625/R-94/003, US Environmental Protection Agency, Washington, D.C.
- Nelson, A.E., Horton, J.W., and Clarke, J.W. 1998. Geologic map of the Greenville quadrangle, South Carolina, Georgia and North Carolina. US Geological Survey, Miscellaneous Investigation Series Map I-2175. Scale 1 : 250 000. 13 pp.
- Nilson, R.H., and Griffiths, S.K. 1983. Numerical analysis of hydraulically-driven fractures. *Computer Methods in Applied Mechanics and Engineering*, **36**: 359–370.
- Pollard, D.D. 1973. Derivation and evaluation of a mechanical model for sheet intrusions. *Tectonophysics*, **19**: 233–269.
- Pollard, D.D., and Holzhausen, G. 1979. On the mechanical interaction between a fluid-filled fracture and the earth's surface. *Tectonophysics*, **53**: 27–57.
- Pollard, D.D., Muller, O.H., and Dockstader, D.R. 1975. The form and growth of fingered sheet intrusions. *Geological Society of America Bulletin*, **86**: 351–363.
- Pollard, D.D., Segall, P., and Delaney, P.T. 1982. Formation and interpretation of dilatant echelon cracks. *Geological Society of America Bulletin*, **93**: 1291–1303.
- Richardson, J. 2003. Forms of hydraulic fractures at shallow depth in Piedmont Soil. M.Sc. thesis, Clemson University, Clemson, S.C. 125 pp.
- Roulier, M., Kemper, M., Al-Abed, S., Murdoch, L., and Davis-Hoover, W. 2000. Feasibility of electrokinetic soil remediation in horizontal Lasagna cells. *Journal of Hazardous Materials*, **B77**: 161–176.
- Savitski, A.A., and Detournay, E. 2002. Propagation of a penny-shaped fluid-driven fracture in an impermeable rock: asymptotic solutions. *International Journal of Solids and Structures*, **39**: 6311–6337.
- Sowers, G.F., and Richardson, T.L. 1982. Residual soils of the Piedmont and Blue Ridge. *Transportation Research Record 919*, National Academy Press, Washington, D.C. pp. 10–20.
- Tan, Q. 2003. Two-dimensional hydraulic fracture simulations using Franc2d. M.Sc. thesis, Clemson University, Clemson, S.C. 153 pp.
- Valko, P., and Economides, M.J. 1995. *Hydraulic fracture mechanics*. Wiley, New York.
- Wahl, H.A., and Campbell, J.M. 1963. Sand movement in horizontal fractures. *Journal of Petroleum Technology*, **15**: 1239–1246.
- Wawrzynek, P., and Ingraffea, A. 1994. FRANC2D: a two-dimensional crack propagation simulator, version 2.7 user's guide. NASA Contractor Report CR-4572, National Aeronautics and Space Administration (NASA), Washington, D.C.
- Wong, R.C.K., and Alfaro, M.C. 2001. Fracturing in low-permeability soils for remediation of contaminated ground. *Canadian Geotechnical Journal*, **38**(2): 316–327.
- Wu, R. 2005. Mechanisms of hydraulic fracturing. Ph.D. dissertation. Georgia Institute of Technology, Atlanta, Ga. 267 pp.
- Zhang, X., Detournay, E., and Jeffrey, R. 2002. Propagation of a penny-shaped hydraulic fracture parallel to the free-surface of an elastic half-space. *International Journal of Fracture Mechanics*, **115**: 125–158.